Searching for non-Abelian phases in the Bose-Einstein condensate of dysprosium

Biao Lian,[1] Tin-Lun Ho,[2] and Hui Zhai[1]

[1]*Institute for Advanced Study, Tsinghua University, Beijing 100084, China*
[2]*Department of Physics, Ohio State University, Columbus, Ohio 43210, USA*

The recently realized Bose-Einstein condensate of dysprosium will become a spin-8 spinor condensate at low magnetic fields. In such a high-spin condensate, many phases with different symmetries can exist. Among them the most interesting ones are those with non-Abelian point group symmetry. In this Rapid Communication we discuss the variety of symmetry phases in a spin-8 condensate resulting from numerical solutions of the Hamiltonian. We show that these symmetries can be determined uniquely from the measurements of density population on each spin component in an ultralow magnetic field, together with the measurements of the collective modes in the zero-field limit. This method can also be applied to Bose-Einstein condensates of other magnetic atoms, such as Cr and Er.

Recently Lev's group has successfully realized the Bose-Einstein condensate of dysprosium (Dy) [1]. Dy is a complex lanthanide atom with a total of 10 f-shell electrons. It has electron spin $S = 2$, orbital angular momentum $L = 6$, and nuclear spin $I = 0$. The total spin $\mathbf{J} = \mathbf{L} + \mathbf{S}$ becomes $J = 8$ due to the Hund's rule. The spin of Dy can be easily polarized by an external magnetic field, which will then give rise to strong magnetic dipolar interactions. However, it is technically possible to reduce the magnetic fields to very low values so that the system is essentially depolarized, as recently achieved in the Cr condensate [2]. In this limit, the spin Hamiltonian has rotational and gauge symmetry, $G = \text{SO}(3) \times \text{U}(1)$. Bose condensation breaks this symmetry. The broken symmetry state has the symmetry of a subgroup of G, which can be either Abelian or non-Abelian. These two types of states are known to have very different properties. For example, while the line defects of Abelian states with different orientation can pass through each other, such a passage is "topologically obstructed" in non-Abelian states, in the sense that a new line defect must be nucleated, connecting the two original ones after they pass through each other [5]. In condensed-matter physics, however, there are very few examples of non-Abelian states. Biaxial nematic liquid crystal probably is the only example [5]. Recently, it has been recognized that cyclic state of spin $S = 2$ condensate [3] is a non-Abelian state [4], and it is expected that the possibilities of non-Abelian states will increase as S increases. High-spin Bose condensates are therefore the most promising systems for finding more examples of non-Abelian states.

At the zero-field limit, the actual spin ground state of Dy is determined by nine scattering lengths that are not yet known. It would be complicated to construct a phase diagram with all these unknown parameters. In this Rapid Communication, we focus on the question of non-Abelian phases of Dy condensate and the simplest scheme to detect them. While the non-Abelian nature of the order parameter is fully manifested in the resulting structure after its line defects cross each other [5], such experiments are too involved in a cold atom setup at present. In this work, we propose a much simpler method to determine the symmetry of a spinor condensate. It combines the measurements of spin populations and the Bogoliubov spectrum. The former can be achieved

with Stern-Gerlach technique while the later can be measured by Bragg spectroscopy. Both techniques are widely used in cold-atom experiments today.

Model. Let $\hat{\psi}_m$ be the bosonic operator for each spin component m, $(m = -J, \ldots, J)$, the Hamiltonian for Dy ($J = 8$) is $\hat{H} = \hat{H}_0 + \hat{H}_{\text{int}}$ [6,7], and

$$\hat{H}_0 = \int d^3\mathbf{r} \sum_{m=-J}^{J} \hat{\psi}_m^\dagger(\mathbf{r}) \left(-\frac{\hbar^2 \nabla^2}{2M} - B g_J \mu_B m \right) \hat{\psi}_m(\mathbf{r}), \quad (1)$$

$$\hat{H}_{\text{int}} = \int d^3\mathbf{r} \sum_{j=0,2,4,\ldots}^{2J} g_j \sum_{m=-j}^{j} \hat{A}_{jm}^\dagger(\mathbf{r}) \hat{A}_{jm}(\mathbf{r}), \quad (2)$$

where $g_j = 2\pi\hbar^2 a_j/M$ and a_j is the s-wave scattering length between a pair of bosons with total spin j, described by the local pair operator $\hat{A}_{jm}(\mathbf{r}) = \sum_{m_1}\langle j,m|J,m_1,J,m-m_1\rangle\psi_{m_1}(\mathbf{r})\psi_{m-m_1}(\mathbf{r})$. Bose statistics, however, implies $j = 0,2,\ldots,16$ only. B is a tiny magnetic field along $\hat{z}$, μ_B is the Bohr magneton, and $g_J = 5/4$ is the Landé g factor for Dy [8].

The energy of a condensate $\langle\psi_{m,\mathbf{k}=0}\rangle = \sqrt{n_0}\varphi_m$ is

$$\mathcal{E} = \sum_{j=0,2,\ldots}^{2J} g_j n_0^2 \sum_m |\mathcal{A}_{jm}|^2 - n_0 B g_J \mu_B \sum_m m|\varphi_m|^2, \quad (3)$$

where $\mathcal{A}_{jm} = \sum_{m_1}\langle j,m|J,m_1,J,m-m_1\rangle\varphi_{m_1}\varphi_{m-m_1}$, while n_0 represents the total density. While there are studies on the scattering of two Dy atoms in a magnetic field [9,10], many scattering lengths a_j are not known at present. We therefore perform a search of the ground state over a vast range of g_j ($j = 0,2,\ldots,2J$) using the imaginary time evolution method. We have also studied the Bogoliubov spectra of these ground states to ensure their stability, which turns out to be very useful for determining their symmetries.

Majorana representation. A very useful way to describe the condensate wave function $\{\varphi_m\}$ is to use the Majorana representation of spin states [11]. Recently, many authors have applied this method to study Bose condensate with high spins [4,12,13]. This representation is most conveniently described in terms of Schwinger bosons [13]. This method presents the spin operators in terms of bosons $\hat{a}$ and $\hat{b}$, such that $\hat{J}_x = (\hat{a}^\dagger\hat{b} + \hat{b}^\dagger\hat{a})/2$, $\hat{J}_y = i(\hat{a}^\dagger\hat{b} - \hat{b}^\dagger\hat{a})/2$,

and $\hat{J}_z = (\hat{a}^\dagger \hat{a} - \hat{b}^\dagger \hat{b})/2$. A general normalized spin state can be written as $|\varphi\rangle = \sum_{m=-J}^{J} \varphi_m |J,m\rangle$, where $|J,m\rangle = [(J+m)!(J-m)!]^{-1/2}\hat{a}^{\dagger J+m}\hat{b}^{\dagger J-m}|0\rangle$. Since the sum in $|\varphi\rangle$ is a homogenous polynomial of $\hat{a}^\dagger$ and $\hat{b}^\dagger$ of degree $2J$, it can be factorized as

$$|\varphi\rangle = \sum_{m=-J}^{J} \varphi_m |J,m\rangle = \frac{1}{\mathcal{N}} \prod_{i=1}^{2J}(u_i \hat{a}^\dagger + v_i \hat{b}^\dagger)|0\rangle, \qquad (4)$$

where $\mathcal{N}$ is a normalization factor to ensure all $|u_i|^2 + |v_i|^2 = 1$. Absorbing the overall phase factor of the product into $\mathcal{N}$, we can write $u_i = \cos(\theta_i/2)$ and $v_i = e^{i\phi_i}\sin(\theta_i/2)$, so that the spinor (u_i, v_i) can be represented as a point on a unit sphere denoted by a unit vector $\hat{\mathbf{n}}_i$ with polar angle (θ_i, ϕ_i). It is straightforward to show that (i) under a spin rotation, $\hat{\mathbf{n}}_i$ rotates as a Cartesian vector and (ii) under time reversal, $(u_i, v_i) \to (v_i^*, -u_i^*)$, which implies $\hat{\mathbf{n}}_i = -\hat{\mathbf{n}}_i$. The $2J+1$ complex numbers $\{\varphi_m\}$ (with totally $4J+1$ real variables because of normalization) are now replaced by $2J$ unit vectors $\hat{\mathbf{n}}_i$ plus an overall phase factor.

Symmetry-allowed states. If U is a rotational symmetry operation, it means the state returns to itself up to an overall phase after being operated on by U, that is, $\varphi_m \to \sum_{m'} U_{mm'}\varphi_{m'} = e^{i\alpha}\varphi_m$. Since the symmetry group G of $\hat{H}$ is $\mathrm{SO}(3) \times \mathrm{U}(1)$, the symmetry of the ground state will be described by one of the normal point groups E, C_n, D_n, T, O, or Y [5]. E is the identity, corresponding to states with no particular symmetry. C_n denotes an n-fold rotational symmetry along certain axis. D_n contains one n-fold C_n axis plus n two-fold C_2 axes perpendicular to C_n. T, O, and Y denote tetrahedral, octahedral, and isocahedral symmetry respectively. The following properties are useful for our later discussions.

(i) If the vectors $\{\hat{\mathbf{n}}_i\}$ come in $(\mathbf{n}, -\mathbf{n})$ pairs, the state is invariant under time reversal.

(ii) A ferromagnetic state (by which we mean $\langle \hat{\mathbf{J}} \rangle \neq 0$) breaks time reversal symmetry and can have only one C_n axis. States with more than one C_n axis such as those with D_n, T, O, and Y symmetry cannot be ferromagnetic, even though they may break time reversal symmetry.

Now let us analyze all the symmetry states:

(1) E: These states have no special symmetry. They are not found as ground states in our energy minimization.

(2) C_n: Dy has $J = 8$, hence 16 points $\hat{\mathbf{n}}_i$ on the unit sphere. So we either have $n \leqslant 16$ or $n = \infty$. The C_n groups can be further classified into C_{nv}, C_{nh}, and S_{2n} [14]. We have found several examples of C_{nv} symmetry. For instance, a C_{5v} state is shown in Fig. 1(a), in which all 16 points form three pentagons and one point sitting at the south pole. However, examples with only C_{nh} or S_{2n} symmetry are not found [15]. We also get states with C_∞ symmetry, with q points ($q < 8$) collapsing into one and other $16 - q$ points into the antipodal point. The case of C_∞ symmetry with $q = 1$ is shown in Fig. 1(b). All the states with C_{nv} and C_∞ symmetry break time reversal symmetry and have ferromagnetic order.

(3) D_n: In this case, either $n = \infty$ or n is a finite integer such that $n \leqslant 16$ for even n, and $n \leqslant 7$ for odd n [16]. D_n symmetry group can be further classified into D_{nd} and D_{nh} [14]. In Figs. 1(c) and 1(d), we show two examples of D_{nd}. D_{8d}
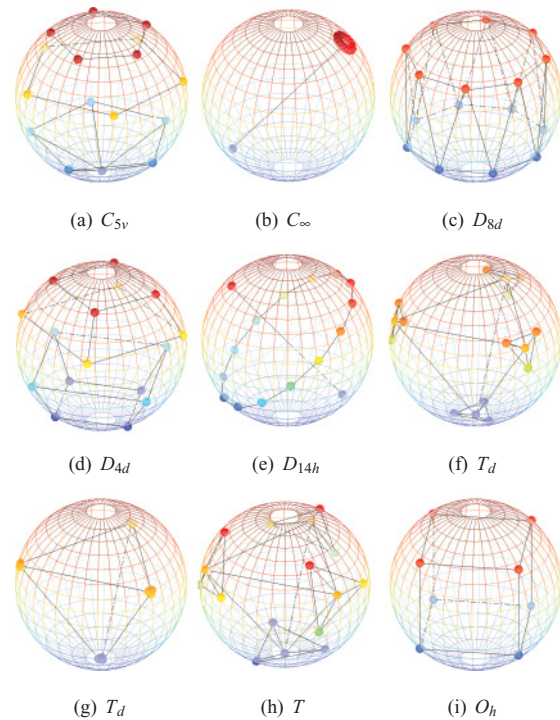

FIG. 1. (Color online) Majorana representations of spin-8 states with different symmetries. Their descriptions are given in the discussion of symmetry-allowed states. The point with polar angle (θ_i, ϕ_i) on the unit sphere represents the spinor $(u_i, v_i) = (\cos\theta_i/2, e^{i\phi_i}\sin\theta_i/2)$.

consists of two octagons, one in the northern hemisphere and the other in the southern hemisphere. D_{4d} consists of four squares, two in the northern hemisphere and the other two in the southern hemisphere. In Fig. 1(e), we show an example of D_{nh}. For D_{14h}, 14 points are evenly distributed on the equator and the other two are placed on the northern and southern poles. While some of these states break time reversal symmetry, such as D_{nd}, none of the states with D_n symmetry are ferromagnetic. However, we do not find the "polar" state with eight points collapsing into the northern pole and the other eight points to the southern pole. We suspect it either does not exist or occupies only a very limited region in the phase diagram.

(4) T: We have found one phase with T symmetry and another with T_d symmetry [14]. They occupy a large portion of the phase diagram. An example of the state with T_d symmetry is shown in Fig. 1(f). Four points are distributed at the vertices of a tetrahedron. Around each tetrahedral vertex, another three points are distributed at equal distance d from it, forming a small regular triangle. The three vertices of this triangle lie in the three mirror planes passing through this tetrahedral vertex. The distance d varies with interaction and can shrink to zero, as shown in Fig. 1(g). We have also found a phase with T symmetry where the vertices of the triangles move away from the mirror plane, as shown in Fig. 1(h). This transition from T_d to T is second order. Both phases T and T_d break time reversal symmetry.

(5) O: This state is described by a cube with two points at each corner, as shown in Fig. 1(i). This state does not break time reversal symmetry and is therefore nonmagnetic.

(6) Y: This is impossible for Dy, as one cannot distribute 16 points on a sphere with icosahedral symmetry. On the other hand, such a phase is possible for Er.

All the states with D_n (n finite), T, or O symmetry have non-Abelian defects [5]. Hereafter we discuss how to detect them experimentally.

Detecting the symmetry. We propose two measurement schemes A and B for probing the symmetry of the system. Scheme A is to measure the population of each spin component after pinning a C_n axis by an ultralow magnetic field along $\hat{z}$. We find numerically that such pinning always happens [8]. The spin wave function along $\hat{z}$ must then be of the form

$$\varphi = (\ldots, 0, \alpha, \underbrace{0, \ldots, 0}_{n-1}, \beta, \underbrace{0, \ldots, 0}_{n-1}, \gamma, 0, \ldots)^T \qquad (5)$$

for any finite n; that is, any nonvanishing component must be separated from the next nonvanishing one by $n-1$ zeros. If $n = \infty$, there will be only one nonzero component. The positions and the magnitudes of the nonvanishing components are also different for different states. This follows from the fact that a spin rotation along $\hat{z}$ axis by $2\pi/n$ will change φ to $e^{i\theta}\varphi$, hence $e^{-i2m\pi/n}\varphi_m = e^{i\theta}\varphi_m$, which can only be satisfied if φ takes the form of Eq. (5).

Scheme B is to detect the low-energy collective modes in zero-field limit using Bragg spectroscopy, which is known to be able to detect low-energy collective modes over the range of wave vector k from 0 to $\sqrt{2m\mu}/\hbar$, where μ is the chemical potential [17]. As explained later, for nonmagnetic states with discrete point group symmetry, there will be a total of four gapless Goldstone modes with linear dispersion. One corresponds to the broken global U(1) symmetry, while the other three correspond to broken spin rotation symmetry. If the remaining symmetry contains only one $C_{n>2}$ axis, two spin rotational modes will be degenerate (i.e., only three different dispersions). If there are more than one $C_{n>2}$ axis, all three rotational modes will be degenerate (i.e., two different dispersions). For ferromagnetic ground states, there will be a quadratic Goldstone mode, as already known from a previous study of magnetism [6]. While these results are found from explicit calculations of the Bogoliubov modes, they in fact result from the following general considerations.

In the low-energy limit $\mathbf{k} \to 0$, the three spin Goldstone modes correspond to simultaneous rotation of all vectors $\hat{\mathbf{n}}_i$ along axes $\hat{x}$, $\hat{y}$, and $\hat{z}$. If there is one $C_{n>2}$ axis, say, along $\hat{z}$, such a rotation transforms the fluctuations along $\hat{x}$ and $\hat{y}$ to those along $\hat{x}'$ and $\hat{y}'$, respectively. Due to the C_n symmetry, the fluctuations along $\hat{x}$ ($\hat{y}$) will behave the same as those along $\hat{x}'$ ($\hat{y}'$). On the other hand, the fluctuations along $\hat{x}'$ or $\hat{y}'$ are linear combinations of those along $\hat{x}$ and $\hat{y}$. It then implies these two modes along $\hat{x}$ and $\hat{y}$ must be degenerate. Furthermore, if there is another $C_{n>2}$ axis, say, along the $\hat{x}$ direction, it will imply that fluctuations along $\hat{y}$ and $\hat{z}$ also have the same dispersion. Then, all three rotational modes are degenerate. These results can be applied to different point groups as summarized in Table I.

Procedures for differentiating different states. Following schemes A and B, we can make the following distinctions.

(i) Distinguishing E and C_n from others: As seen in Table I, these are the only two ferromagnetic states, and thus

TABLE I. Illustration of collective modes of different symmetry states. L and Q stand for modes linear and quadratic in k respectively; "2(3) dg." is short for two (three) degenerate modes.

Symmetry	Phase mode	Spin modes	Distinct dispersions
E	$1L$	$1L + 1Q$	$2L + 1Q$
C_n	$1L$	$1L + 1Q$	$2L + 1Q$
D_n	$1L$	$3L$ (2 dg.)	$3L$
T, O	$1L$	$3L$ (3 dg.)	$2L$
D_∞	$1L$	$2L$ (2 dg.)	$2L$

they have quadratic Goldstone modes. The case of C_{5v} is show in Fig. 2(a). Thus, scheme B can distinguish them from other states. Moreover, E and C_n can be distinguished and determined by scheme A, as C_n has the characteristic order parameter as shown in Eq. (5). (Note that our calculations show that an external magnetic field always pins the C_n axis of C_n states.)

(ii) Distinguishing D_n from D_∞, T, and O: As seen in Table I, D_n differs from T and O from the number of mode velocities. [See also Figs. 2(b)–2(d)]. In scheme A, a very low magnetic field pins along $\hat{z}$ either the C_n or C_2 axis of the D_n symmetry, depending on the states [8]. If the C_2 axis is pinned, then we can add a small magnetic field gradient $\mathbf{B} = B[\hat{z} + G_0(x\hat{x} - z\hat{z})]$. This is effectively equivalent to adding an energy $\epsilon\langle F_y^2\rangle$, with $\epsilon = \hbar^2 G_0^2/(2M)$ [18], which will pin the C_n axis along either the $\hat{x}$ or $\hat{y}$ direction. One can then determine n by measuring the spin population along $\hat{x}$ or $\hat{y}$ [8].

(iii) Distinguishing D_∞, T, and O: Our calculations show an ultralow magnetic field always pins the C_3 axis of T symmetry and pins the C_4 axis of the O state. Even though our calculations did not find the "polar" state with D_∞ symmetry, we note that if present, it can be pinned only along either the C_∞ or the C_2 axis by magnetic field, which is distinct from T and O. So by scheme A we can easily distinguish these three. Another difference between T and O is that the T phase breaks time reversal symmetry, while the O phase does not. Hence for
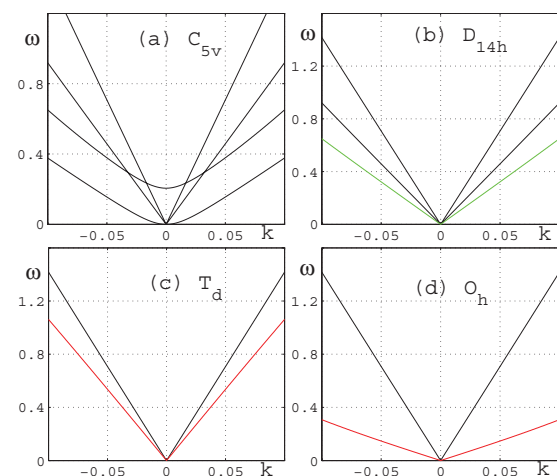

FIG. 2. (Color online) Low-energy spectra of Bose condensates with different symmetries. k is in units of $k_0 = \sqrt{2m\mu}/\hbar$ and ω is in units of 0.1μ (μ: chemical potential). The green (red) line stands for two (three) degenerate modes. See also Table I.
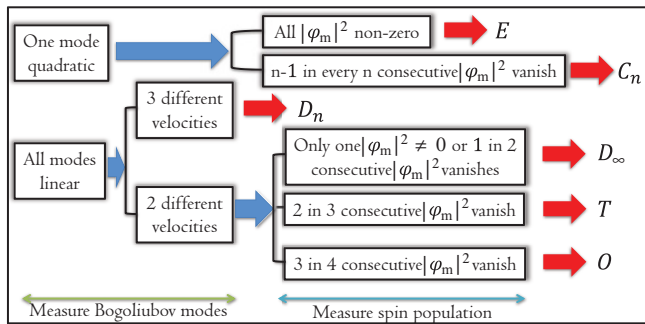
FIG. 3. (Color online) Procedures for determining the symmetry of different phases. Blue and red arrows denote the measurement of collective modes and spin populations $|\varphi_m|^2$ respectively.

the O phase, we have $|\varphi_m|^2 = |\varphi_{-m}|^2$ in the zero-field limit, which is a property not shared by the T phase [8].

In Fig. 3 we summarize our proposal with a flow diagram. Following these steps, all possible (normal point group) symmetries can be determined exactly.

Final comments. Although our discussions are for Dy, our method of detection is applicable for all spinor condensates such as Cr [2] and Er [19]. In our discussion, we have not considered dipole energy. The competition between dipole energy and spin-dependent s-wave interaction will certainly change the energetics. However, dipolar energy is known to depend strongly on the geometry of the trap and to have less effect in spherical potentials. Moreover, since all the non-Abelian states are nonmagnetic, dipolar interaction may not have strong effects on them. In settings where dipolar interaction becomes dominant, the system tends to develop nonuniform spin textures as shown in the recent experiments on ^{87}Rb [20]. Even in such cases, the underlying zero-field states such as those discussed here still play an important role in determining the global equilibrium spin textures [21].

[1] M. Lu, N. Q. Burdick, S. H. Youn, and B. L. Lev, Phys. Rev. Lett. **107**, 190401 (2011).

[2] B. Pasquiou, E. Marechal, G. Bismut, P. Pedri, L. Vernac, O. Gorceix, and B. Laburthe-Tolra, Phys. Rev. Lett. **106**, 255303 (2011).

[3] C. V. Ciobanu, S.-K. Yip, and T.-L. Ho, Phys. Rev A **61**, 033607 (2000).

[4] R. Barnett, A. Turner, and E. Demler, Phys. Rev. Lett. **97**, 180412 (2006).

[5] See Secs. V and VI of the review article by N. D. Mermin, Rev. Mod. Phys. **51**, 591 (1979).

[6] T. L. Ho, Phys. Rev. Lett. **81**, 742 (1998).

[7] T. Ohmi and K. Machida, J. Phys. Soc. Jpn. **67**, 1822 (1998).

[8] See Supplemental Material at http://link.aps.org/supplemental/10.1103/PhysRevA.85.051606 for more details.

[9] S. Kotochigova and A. Petrov, Phys. Chem. Chem. Phys. **13**, 19165 (2011).

[10] A. Petrov, E. Tiesinga, and S. Kotochigova, arXiv:1203.4172 (2012).

[11] E. Majorana, Nuovo Cimento **9**, 43 (1932).

[12] A. Lamacraft, Phys. Rev. B **81**, 184526 (2010); Y. Kawaguchi and M. Ueda, Phys. Rev. A **84**, 053616 (2011); M. Fizia and K. Sacha, J. Phys. A: Math. Theor. **45**, 045103 (2012); H. Mäkelä and K.-A. Suominen, Phys. Rev. Lett. **99**, 190408 (2007).

[13] R. Barnett, D. Podolsky, and G. Refael, Phys. Rev. B **80**, 024420 (2009).

[14] C_{nv} is C_n plus n vertical mirror planes, C_{nh} is C_n plus a horizontal mirror plane, and S_{2n} is generated by a π/n rotation combined with a horizontal mirror reflection. Operating S_{2n} twice will result in a C_n rotation. D_{nh} is D_n plus a vertical mirror plane containing a C_2 axis. D_{nd} is D_n plus a vertical mirror plane between two C_2 axes. T_d is T plus a mirror plane that dissects the tetrahedron evenly. O_h is O plus inversion. See J. P. Elliott and P. G. Dawber, *Symmetry in Physics* (Oxford University Press, New York, 1986).

[15] C_{nh} and S_{2n} are subgroups of D_{nh} and D_{nd} respectively. States with C_{nh} (S_{2n}) symmetry but no D_{nh} (D_{nd}) are never found in calculations.

[16] If n is odd and $2n > 16$, then there must be n points on the equator. The other $16 - n$ points can only be put into the northern or southern pole to satisfy C_n symmetry. However, since $16 - n$ is odd, these points cannot be distributed evenly at the two poles, making it impossible to have D_n symmetry.

[17] D. M. Stamper-Kurn, A. P. Chikkatur, A. Görlitz, S. Inouye, S. Gupta, D. E. Pritchard, and W. Ketterle, Phys. Rev. Lett. **83**, 2876 (1999).

[18] T. L. Ho and S. K. Yip, Phys. Rev. Lett. **84**, 4031 (2000).

[19] Laser cooling has been made for Er: A. J. Berglund, J. L. Hanssen, and J. J. McClelland, Phys. Rev. Lett. **100**, 113002 (2008); K. Aikawa, A. Frisch, M. Mark, S. Baier, A. Rietzler, R. Grimm, and F. Ferlaino, arXiv:1204.1725.

[20] M. Vengalattore, S. R. Leslie, J. Guzman, and D. M. Stamper-Kurn, Phys. Rev. Lett. **100**, 170403 (2008).

[21] J. Zhang and T. L. Ho, J. Low Temp. Phys. **161**, 325 (2010).